Virology 387 (2009) 11–15

Contents lists available at ScienceDirect

Virology

journal homepage: www.elsevier.com/locate/yviro

Rapid Communication

Single-particle cryo-electron microscopy of Rift Valley fever virus

Michael B. Sherman [a,b,1], Alexander N. Freiberg [c,d,1], Michael R. Holbrook [c,d,e], Stanley J. Watowich [a,b,d,e,*]

[a] Department of Biochemistry and Molecular Biology, University of Texas Medical Branch, Galveston, TX 77555, USA
[b] Sealy Center for Structural Biology and Molecular Biophysics, University of Texas Medical Branch, Galveston, TX 77555, USA
[c] Department of Pathology, University of Texas Medical Branch, Galveston, TX 77555, USA
[d] Center for Biodefense and Emerging Infectious Diseases, University of Texas Medical Branch, Galveston, TX 77555, USA
[e] Institute for Human Infections and Immunity, University of Texas Medical Branch, Galveston, TX 77555, USA

ARTICLE INFO

Article history:
Received 26 January 2009
Returned to author for revision
13 February 2009
Accepted 25 February 2009
Available online 21 March 2009

Keywords:
Bunyaviridae
Rift Valley fever virus
Cryo-electron microscopy
Single-particle averaging
Inter-capsomer contacts

ABSTRACT

Rift Valley fever virus (RVFV; *Bunyaviridae*; *Phlebovirus*) is an emerging human and veterinary pathogen causing acute hepatitis in ruminants and has the potential to cause hemorrhagic fever in humans. We report a three-dimensional reconstruction of RVFV vaccine strain MP-12 (RVFV MP-12) by cryo-electron microcopy using icosahedral symmetry of individual virions. Although the genomic core of RVFV MP-12 is apparently poorly ordered, the glycoproteins on the virus surface are highly symmetric and arranged on a $T=12$ icosahedral lattice. Our RVFV MP-12 structure allowed clear identification of inter-capsomer contacts and definition of possible glycoprotein arrangements within capsomers. This structure provides a detailed model for phleboviruses, opens new avenues for high-resolution structural studies of the bunyavirus family, and aids the design of antiviral diagnostics and effective subunit vaccines.

Introduction

Rift Valley fever virus (RVFV) is the prototypical *Phlebovirus* (family *Bunyaviridae*) associated with large severe disease outbreaks throughout Africa and within the Arabian Peninsula (Balkhy and Memish, 2003). Infection of livestock can result in economically disastrous spontaneous abortions with a high mortality among young animals. Human infection is primarily a self-limiting febrile disease; however 1–2% of infected individuals develop serious complications including retinitis, hepatitis, encephalitis, hemorrhagic fever, and death (Schmaljohn and Nichol, 2007). Similar to most bunyaviruses, RVFV is a spherical virus with a lipid-membrane envelope and surface protrusions believed to be composed of two viral transmembrane glycoproteins. RVFV contains a tripartite, single stranded, negative-sense RNA genome. The L(arge) RNA segment encodes the RNA-dependent RNA polymerase L, while M(edium) RNA segment encodes the NSm non-structural protein, G_N (54 kDa) and G_C (59 kDa) glycoproteins, and the 78 kDa protein (comprising the entire NSm and G_N proteins). The phlebovirus S(mall) segment uses an ambisense strategy to encode the nucleoprotein N and non-structural protein NSs. The three RNA segments each bind N and L proteins to form ribonucleoprotein (RNP) complexes that are contained within the interior of the virus particle. To better understand the structural organization of this virus family, we recently completed a cryo-electron tomographic (cryo-ET) reconstruction of individual RVFV MP-12 particles (Freiberg et al., 2008). Unexpectedly, that work showed that RVFV was a spherical virus containing regularly spaced glycoprotein protrusions arranged as capsomers on an icosahedral $T=12$ lattice. Since our cryo-ET reconstruction of RVFV MP-12 showed the virus assembled into icosahedral particles (Freiberg et al., 2008), we performed a single-particle image processing of RVFV MP-12 that generated a 27 Å resolution three-dimensional (3D) map of the virus. This reconstruction revealed new structural features of the glycoprotein capsomers and the contacts between adjacent capsomers. The glycoprotein interactions observed within and between capsomers likely direct the icosahedral assembly of RVFV. Our reconstruction demonstrates that members of the *Phlebovirus* genus, and perhaps all bunyaviruses, assemble into icosahedral particles, contrary to the previously accepted belief that these viruses are pleiomorphic.

Results

Icosahedral reconstruction of RVFV MP-12

When examined by cryo-electron microscopy (cryo-EM), RVFV MP-12 particles appeared round with a majority having the same

* Corresponding author. Department of Biochemistry and Molecular Biology, University of Texas Medical Branch, Galveston, TX 77555-0647, USA. Fax: +1 409 747 4745.
E-mail address: watowich@xray.utmb.edu (S.J. Watowich).
[1] These authors contributed equally.

0042-6822/$ – see front matter © 2009 Elsevier Inc. All rights reserved.
doi:10.1016/j.virol.2009.02.038

diameter. Many particles had pronounced regular spikes at the outer circumference of the virus. The diameter of the virus particles was ~1000 Å, consistent with our recent cryo-ET reconstruction (Freiberg et al., 2008). A total of 381 particle images were boxed out of 93 CCD frames and used for initial 3D reconstruction. Several origin/orientation refinement cycles were performed leading to stable 3D map of RVFV MP-12 virions. Images inconsistent with the majority of the dataset were discarded from further processing; the final 3D map with an effective resolution of 27 Å was reconstructed from the 108 best virus images (Fig. 1). Although our RVFV MP-12 3D map contained a modest number of particles, averaging using the particle's icosahedral symmetry resulted in a significant reduction of noise that allowed for clear delineation of capsomer morphology and the lipid bilayer (Fig. 1).

Glycoprotein arrangement in RVFV

The 3D map of RVFV MP-12 (Fig. 1) clearly showed $T=12$ icosahedral symmetry. The symmetry was consistent with previous cryo-ET studies of RVFV and Uukuniemi virus (UUKV) (Freiberg et al., 2008; Overby et al., 2008). The two glycoproteins, G_N and G_C, were organized in 122 distinct capsomers on the virus surface, extending ~96 Å above the lipid envelope (Fig. 1). There were 12 pentameric (pentons) and 110 hexameric (hexons) protrusions. Each capsomer resembled a hollow cylinder formed by a tight association between viral glycoproteins. The pentons and hexons were interconnected by ridges of protein density located close to the lipid envelope (blue arrow in Fig. 1A). As a consequence of the $T=12$ symmetry, three quasi-equivalent types of hexons (labeled A, B, C in Fig. 1A) were distinguished in the map. These capsomers (not related to each other by icosahedral symmetry) were located on the icosahedral 2-fold, 3-fold, and quasi 3-fold axes of symmetry, respectively. The maps in Fig. 1 were colored by radius according to the scale bar at the lower right corner. Fig. 1B shows concentric shells of envelope proteins, lipid bilayer, and core region of RVFV MP-12. The G_N/G_C glycoprotein shell is shown in gold (radial range ~430 Å to ~530 Å), lipid envelope in green (~375 Å to ~430 Å), and RNP core in red (0 Å to ~355 Å). The RNP core was separated from the inner surface of the envelope by a ~20 Å gap.

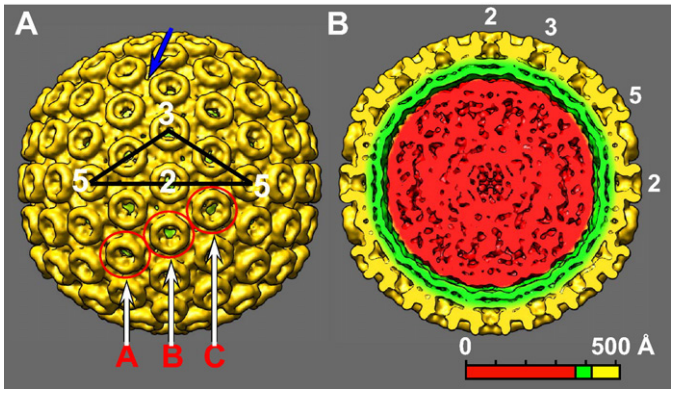

Fig. 1. Cryo-EM 3D map of RVFV MP-12. (A) Surface-shaded representation of the map rendered at 1 standard deviation (1σ) showing glycoprotein protrusions organized with $T=12$ icosahedral symmetry, so far unique to the *Bunyaviridae* family. The black triangle demarks an asymmetric unit with 5-, 3- and 2-fold axes indicated. There are 12 pentons in the map and 110 quasi-equivalent hexons of three types: A-, B-, and C, occupying locations at 2-, 3- and quasi-3-fold axes, respectively. The blue arrow points to a ridge connecting two capsomers. (B) Surface-shaded representation as in panel (A) with front half of the map removed to reveal interior features. The map was colored by radius and the structure consists of an outer glycoprotein layer (gold), a lipid envelope (green), and a ribonucleoprotein core (red). Icosahedral two- (2), three- (3), and five-fold (5) axes are labeled. The core is separated from the envelope by a ~20 Å gap and details in the core are not resolved because of its asymmetry. Images are colored radially, according to the scale bar.

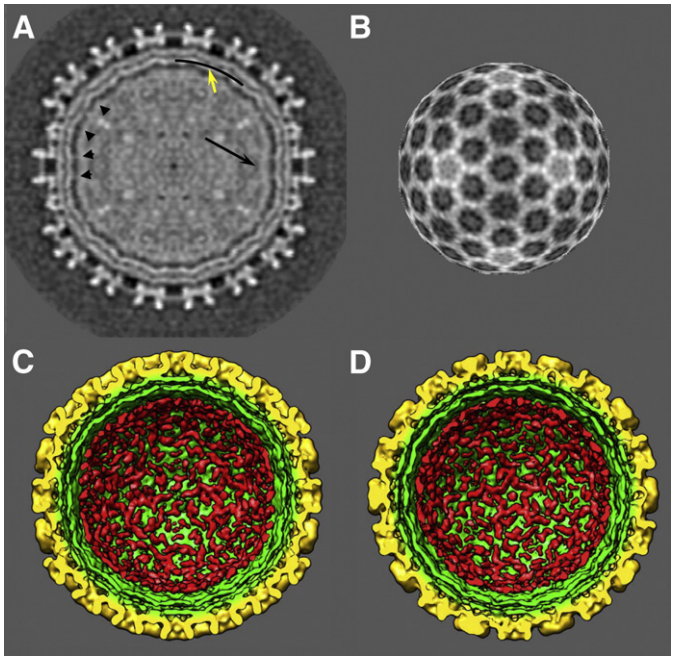

Fig. 2. The lipid bilayer and glycoprotein-RNP core interactions. (A) A central section through the RVFV MP-12 map showing glycoprotein protrusions at the surface of the virions, double-layered lipid envelope acquired during budding of virus particles and unstructured core. The black arrow points to an underlying higher density layer, which might represent a higher occupancy layer where RNP segments are tethered by cytoplasmic tails of G_N and G_C glycoproteins. Arrowheads point to connecting densities protruding through the envelope, most likely representing glycoprotein cytoplasmic tails. Protein is shown in white and the map is in 2-fold orientation with one 2-fold axis pointing towards the reader. The black arc and yellow arrow represent the radius of radial projection shown in panel (B). (B) Radial projection of RVFV MP-12 map at 378 Å radius showing protein densities traversing the lipid envelope. Protein is shown in white. (C and D) Surface-shaded representation of the map rendered at 1.5σ with front half of the map removed to reveal interior features. Details in the RNP core are not resolved because of its asymmetry but in the closest to envelope layer short fibril-like features are seen. These fibrils could represent pieces of RNP segments in the core. They "survived" icosahedral averaging because of interactions with icosahedral glycoprotein shell through the densities traversing the envelope. The map is shown in 2-(C) and 5-fold (D) orientations.

The lipid envelope and glycoprotein-RNP core interactions

The viral envelope is clearly visible in Figs. 1B and 2 as ~50 Å wide ring, which was in good agreement with our tomographic reconstruction (Freiberg et al., 2008). Since bunyaviruses do not have a capsid or matrix protein located inside the lipid envelope, the glycoprotein cytoplasmic tail domains (CTDs) have been proposed to facilitate interactions between the RNP core and the glycoproteins (Overby et al., 2007; Shi et al., 2007). Individual RNP segments were not resolved in the current reconstruction, because they were not arranged with icosahedral symmetry and therefore were averaged out in the reconstruction. The RNP core was separated from the inner surface of the envelope by a ~20 Å gap. We observed connecting densities from outer glycoprotein layer that spanned the envelope traversing the gap and pointing to the core (e.g., Fig. 2A, arrowheads). These connecting densities represent glycoprotein CTDs interacting with RNPs or other proteins in the core. Interestingly, at a radius of 378 Å (just outside of the inner leaflet of the envelope) a striking pattern of protein densities was detected (Fig. 2B). Obviously, these higher-than-lipid densities represent glycoprotein CTDs that penetrate the envelope and link glycoprotein ecto-domains with RNPs in the core. The CTDs extending from pentons (bright five-fold regions in Fig. 2B) are brighter than the tails extending from hexons because pentons are positioned differently from hexons. However, both pentons and hexons clearly provide tethers for RNPs (Figs. 2A, arrow, C and D, red fibril-like features).

Capsomer morphology

A- and B-type hexons (Fig. 1A) and a penton were computationally extracted from the virus map for direct structural comparison (Fig. 3). The hexons had similar dimensions, although slight differences in their shape were observed due to the different environments resulting from the $T=12$ organization (Figs. 3A and B). Each hexon was a hollow cylindrical protrusion with outer and inner diameters of 125 Å and ~84 Å, respectively, and a height of ~96 Å. The hexon volume was calculated to be ~1,300,000 Å^3 (including part of base layer just above the lipid bilayer and extending half-way between the capsomers), equivalent to a ~1100 kDa protein. Most likely, the hexons are composed of G_N/G_C multimers. A constriction was visible in the interior of the hexons at a height of ~65 Å from the lipid membrane. This constriction had an interior diameter of ~40 Å and did not block access to the interior cavity of the capsomers (Figs. 3A, B, D, and E).

The hexons had six globules in their upper rim (Fig. 3A, circled), suggesting large glycoprotein domains (Figs. 3A and B). Halfway between the rim and the bilayer directly below the globules there were ridges of density that connected capsomers. Inside these ridges we found channels of ~18 Å in diameter running between adjacent capsomers interconnecting their inner cavities (arrows in Figs. 3C and E). The lipid envelope formed the base of these channels. Although the inter-capsomer ridges were previously observed in cryo-ET reconstructions of RVFV MP-12 (Freiberg et al., 2008) and UUKV (Overby et al., 2008), the current higher resolution reconstruction allowed identification of the channels inside the ridges. At higher density thresholds, the upper rim of a hexon was clearly visible with strands of density twisting counterclockwise (as viewed from the outside) and downwards from the capsomer rim toward the base of the capsomer (Fig. 3F, arrows).

Pentons were more compact than hexons with an outer diameter of ~120 Å and an inner diameter of ~65 Å (Fig. 3G). The penton volume (including part of the floor similar to hexons) was calculated to be ~1,000,000 Å^3, equivalent to a protein of mass of 840 kDa, again most likely composed of G_N/G_C multimers. Unlike the hexons, the space inside the penton was divided by a plug positioned at ~58 Å outward from the penton base (Fig. 3H, black arrow). This density plug partitioned the penton's inside into an isolated inner cavity and an external caldera. Open channels were located at the base of the capsomer and extended horizontally from the inner cavity of the penton to adjacent hexons (Fig. 3H, white arrow). When the map was rendered at a higher threshold, helical strands of density were observed extending clockwise (as viewed from the outside) and

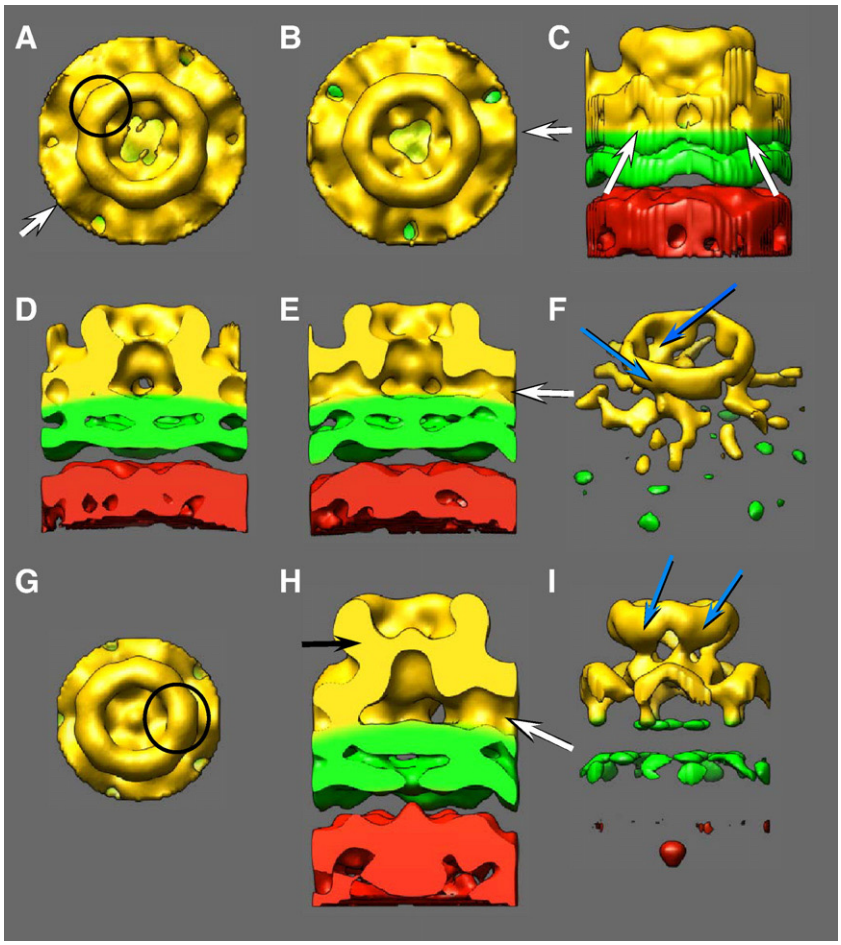

Fig. 3. Glycoprotein arrangement in hexons and pentons. (A–F) Hexameric, (G–I) pentameric capsomers cut from the 3D cryo-EM map of RVFV MP-12. Top views of A-type hexon at 2-fold location (A), and of B-type hexon at 3-fold location (B), with constrictions visible inside the calderas (see text). Arrows point to the side channels inside ridges. Six globules in the upper rim are visible in both capsomers (one is circled). They may represent large domains of G_N/G_C glycoproteins. (C) Side view of a B-type hexon shown in panel (B). Arrows point to two different side channels running to adjacent capsomers in the structure. Hexons (gold) protrude by ~96 Å outwards from the envelope (green); the density corresponding to the RNP core is shown in red. (D) Side view of A-type hexon (panel (A)) with front half removed to show the central cavity. Constriction is clearly seen at ~65 Å from the bottom. (E) Same as (D) but for B-type hexon (panel (B)) showing side channels on both sides of the capsomer (white arrow). (F) Tilted view of a B-type hexon rendered at higher threshold to highlight helical arrangement of ridges connecting upper rim to lower portion of the hexon (blue arrows). (G) Top view of a penton. Five globules around the upper rim are visible (one is circled). Similar to hexons they may represent large G_N/G_C domains. The central plug inside the cavity is visible. The plug is more massive compared to constriction seen in hexons. (H) Side view of the penton with front half removed to show central cavity below the plug (black arrow) and side channel of ~18 Å in diameter (white arrow). (I) The penton rendered at higher density threshold showing a dense rim on top and helically arranged ridges connecting the rim to lower part of the penton (arrows), analogous to (F).

downward from the inner surface of the penton rim (arrows in Fig. 3I). These helical strands, also described for hexons (Fig. 3F), possibly represent glycoprotein stalk regions/domains which might be involved in formation of capsomers and/or ridges.

Inter-capsomer interactions

The present reconstruction revealed new structural features of the capsomers and the contacts between adjacent capsomers. At a radius of 447 Å, which was ~10 Å above the lipid envelope, a network of channels appeared to interconnect all individual capsomers (Fig. 4A, black lines). These channels run within ridges that link adjacent capsomers (Figs. 1A, blue arrow, and 4C, black arrows). Central cavities of neighboring capsomers (Fig. 4C, red arrows) connected by channels (in Fig. 4C, white arrows) are clearly visible. The ridges make robust links between capsomers and are comparable in density to glycoprotein interactions within capsomers (Fig. 4C). These ridges represent inter-capsomer interactions that could play an important role in virus assembly and stability.

Glycoprotein structure

Atomic resolution structures of bunyavirus glycoproteins are unknown, and their similar molecular masses of 54 kDa (G_N) and 59 kDa (G_C) make it difficult to reliably locate the G_N and G_C glycoproteins separately within the RVFV structure. We therefore estimated capsomer volumes of pentons and hexons to be ~840 and ~1100 kDa, respectively, suggesting pentons could accommodate 10 glycoprotein molecules and hexons would contain 12. For capsomer volumes estimated in this study, the floor layer (i.e., density immediately above the lipid bilayer and colored gold in Fig. 3C) was included in the measurements, resulting in higher values compared to calculations from our previous cryo-ET reconstruction (Freiberg et al., 2008). The limited resolution of the RVFV MP-12 structure, the similar molecular mass of G_N and G_C glycoproteins, and lack of RVFV glycoprotein atomic resolution structures made it impractical to unambiguously locate individual glycoproteins within capsomers. However, a sequence alignment of the phlebovirus G_C glycoprotein and the alphavirus E1 glycoprotein suggested both proteins would adopt a similar three-domain structure (Garry and Garry, 2004). We could use that homology at higher EM resolutions to locate the glycoproteins within capsomers.

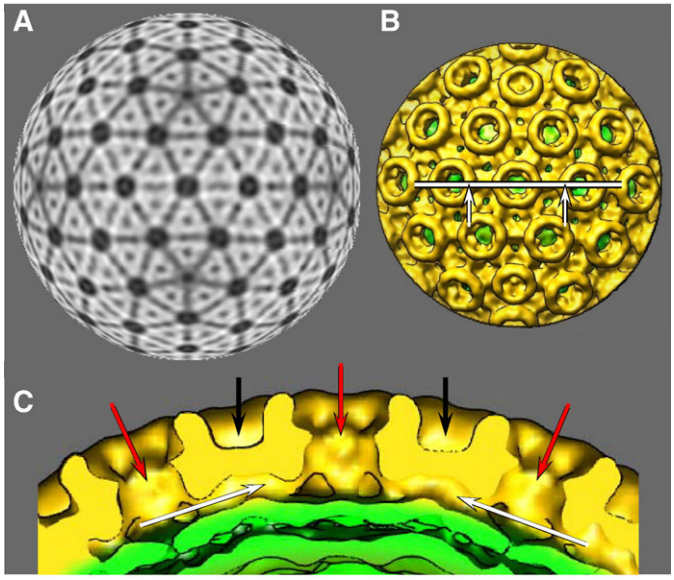

Fig. 4. Capsomer interactions. (A) Radial projection of RVFV MP-12 map at 447 Å radius showing network of channels running between capsomers (black lines). The channels interconnect all the capsomers internal cavities. Protein densities are represented in white. The projection is shown in 2-fold orientation. (B) Fragment of the map showing several capsomers. The white line represents the cut through the map shown in panel C. (C) 90° rotated view of three central hexons (as indicated in panel B) with front half removed. Red arrows mark cavities in individual hexons. Strong connecting densities (ridges) between capsomers are indicated by black arrows. Interconnecting channels are denoted by white arrows.

Discussion

This study presents icosahedral 3D reconstruction of a virus within the large *Bunyaviridae* family. The reconstruction provides a foundation of using symmetry to determine phlebovirus structures at increasingly higher resolutions. Combined with the UUKV structure (Overby et al., 2008) these data demonstrate that Phleboviruses adopt an icosahedral structure. Ultimately, high-resolution structures of viruses from each of the five genera will allow a detailed understanding of structure–function relationship of these viruses and identify differences and similarities between diverse members of the *Bunyaviridae* family.

The structure of RVFV (vaccine strain MP-12; genus *Phlebovirus*) was determined to 27 Å resolution and enabled detailed structural features to be delineated. The viral glycoproteins were clearly arranged on an icosahedral lattice with a triangulation number of $T = 12$. To date, this arrangement has only been described for RVFV and UUKV, both members of the *Phlebovirus* genus (Freiberg et al., 2008; Overby et al., 2008). The capsomer volumes suggest the hexons and pentons contain 12 and 10 glycoproteins, respectively. Although the exact composition and location of individual G_N and G_C glycoproteins within the capsomers cannot be resolved in the current structure, biochemical data suggested the RVFV glycoproteins form G_N/G_C heterodimers with approximately similar amounts of G_N and G_C incorporated into the virion (Gerrard and Nichol, 2007). However, RVFV glycoproteins may also form homodimers, since homodimers have been described for the related phleboviruses Punta Toro virus (homodimers of G_C) and UUKV (homodimers of G_N or G_C) (Chen and Compans, 1991; Ronka et al., 1995). Extensive inter- and intra-capsomer interactions observed on the RVFV surface suggest that the glycoprotein multimers may participate in RVFV assembly. The globules observed within each capsomer could be formed by glycoprotein heterodimers, where one glycoprotein of the dimer forms intra-capsomer contacts and the second glycoprotein extends outward to form the inter-capsomer contacts; these channels could form from “head-to-tail” homodimers reminiscent of the E1 dimers observed in alphaviruses. The G_C of *Bunyaviridae* has been predicted to be a class II fusion peptide as is the alphavirus E1 and flavivirus E protein (Garry and Garry, 2004; Rey et al., 1995). Determining the detailed arrangement of the envelope glycoproteins within capsomers will require higher resolution structures. These studies would be aided by glycoprotein-specific monoclonal antibody labeling and atomic resolution structures of the glycoproteins which will allow pseudo-atomic models of the outer shell of RVFV to be constructed.

The outer glycoprotein shell of RVFV was separated from the RNP core by a lipid bilayer. The densities that traverse the bilayer might represent regions of interaction between the glycoprotein CTDs and the RNP components lining the inner surface of the lipid envelope (Figs. 2A and B). These densities were likely the G_N CTDs, which were predicted to contain 82 amino acids in contrast to the smaller G_C CTDs assumed to contain only 16 amino acids (http://www.cbs.dtu.dk/services/TMHMM-2.0). The putative RVFV G_N CTD densities were observed to extend into the RNP core (Figs. 2C and D), which was consistent with biochemical data indicating that G_N CTDs from Bunyamwera virus (BUNV, *Orthobunyavirus* genus) and related UUKV were necessary for genome packaging (Overby et al., 2007; Shi et al., 2007).

The absence of a bunyavirus capsid or matrix protein suggests that capsomer–capsomer interactions play a central role in defining the

icosahedral structure of RVFV. Highlighting the importance of inter-glycoprotein contacts for virus assembly, Overby et al. demonstrated that empty UUK virus-like particles (VLPs) could be generated from expressed G_N and G_C glycoproteins (Overby et al., 2006); however, the detailed structure of these particles was not established. RVF VLPs have also been generated either from expressed G_N, G_C and nucleoprotein (N) or expressed G_C and N proteins (Liu et al., 2008), although the latter VLPs were found to be more pleiomorphic than VLPs containing both glycoproteins. These data suggest that the G_C glycoprotein is primarily responsible for intra-capsomer interactions, with G_N mediating inter-capsomer interactions necessary to define the icosahedral structure.

The results presented in this study will lead to a better understanding of the assembly process and overall structure of phleboviruses and bunyaviruses in general. An understanding of glycoprotein arrangement within the virus and their intra- and inter-capsomer interactions (indicating their importance for virus assembly/disassembly and stability) will help to rationally develop conformationally-specific subunit vaccines.

During review and revision of this manuscript, a complementary cryo-electron microscopy study of glutaraldehyde-fixed RVFV clone 13 was accepted for publication (Huiskonen et al., in press). Single-particle image processing was used in both cases and gave similar results.

Materials and methods

Cryo-electron microscopy and image processing

Concentration and purification of RVFV MP-12 has been performed as described (Freiberg et al., 2008). RVFV MP-12 virions were vitrified as previously described (Freiberg et al., 2008) on Quantifoil grids (R2×2 Quantifoil®; Micro Tools GmbH, Jena, Germany) and imaged in a JEOL 2200FS microscope operated at 200 keV using 40,000× EM magnification. Image acquisition was done using a 4k×4k slow-scan CCD camera (UltraScan 895, GATAN, Inc.). An in-column omega electron energy filter was used during imaging with zero-loss energy peak selected with 20 eV slit. Images were acquired with ~20 electrons/Å^2 dose; pixel size corresponded to 3 Å on the specimen scale. We used 0.7–3.7 μm defocus range for imaging with majority of images taken at 1.5–2.5 μm underfocus.

Individual virion images were boxed from CCD frames using BOXER program from the EMAN suite (Ludtke et al., 1999). Icosahedral image processing software developed in T. S. Baker's lab (http://cryoem.ucsd.edu/programs.shtm) was used for contrast transfer function (CTF) determination, particle alignment, and projection matching. Selected images of individual RVFV MP-12 virions were corrected for CTF of the microscope.

An icosahedron matching the size of RVFV MP-12 particles was used as an initial model for orientation search and first alignment of the images (Baker and Cheng, 1996). With only few RVFV MP-12 particle images chosen manually from the dataset, we obtained a map that resembled our cryo-ET reconstruction (Freiberg et al., 2008) and used that for subsequent origin and orientation search for the whole dataset. Orientation/origin refinement was done using a modified version of the PFT protocol (Zhang et al., 2003). Several origin/orientation refinement cycles were performed leading to stable 3D map of the RVFV MP-12 virions. At the same time, no further improvement in resolution was observed and refinement was stopped at that point. At each iteration step all images were aligned relative to the projections of the 3D map obtained in previous search/refinement cycles. Best images were then selected to calculate a new 3D map which was used as the reference for next round of refinement. The final 3D map was reconstructed from the 108 best virion images. Effective resolution of the map was 27 Å according to 0.5 Fourier shell correlation function (FSC) criterion.

3D density maps were calculated using P3DR (Ji et al., 2006). We used PSF (Ji et al., 2006) to calculate FSC; the resolution of the reconstruction was determined using a conservative threshold of 0.5 (Rosenthal and Henderson, 2003). Since the RNP core lacked icosahedral order, it was excluded from FSC calculations. The 3D maps were surface-rendered and displayed with one standard deviation (1σ) threshold in ROBEM and CHIMERA (Pettersen et al., 2004), which theoretically accounted for ~100% particle volume. Capsomer volumes and molecular mass were calculated using a value of 0.844 Da/Å^3 for protein density (Matthews, 1968).

Acknowledgments

We thank Drs. C.J. Peters and Shinji Makino for helpful discussions. This work was supported by a training fellowship from the W. M. Keck Foundation to the Gulf Coast Consortia through the Keck Center for Virus Imaging (A.N.F.), and by grants from the NIH/NIAID Western Regional Center of Excellence for Biodefense and Emerging Infectious Disease Research (sub-award from U54 AI057156 to M.B.S.) and the Welch Foundation (S.J.W.).

References

Baker, T.S., Cheng, R.H., 1996. A model-based approach for determining orientations of biological macromolecules imaged by cryoelectron microscopy. J. Struct. Biol. 116 (1), 120–130.
Balkhy, H.H., Memish, Z.A., 2003. Rift Valley fever: an uninvited zoonosis in the Arabian peninsula. Int. J. Antimicrob. Agents 21 (2), 153–157.
Chen, S.Y., Compans, R.W., 1991. Oligomerization, transport, and Golgi retention of Punta Toro virus glycoproteins. J. Virol. 65 (11), 5902–5909.
Freiberg, A.N., Sherman, M.B., Morais, M.C., Holbrook, M.R., Watowich, S.J., 2008. Three-dimensional organization of Rift Valley fever virus revealed by cryoelectron tomography. J. Virol. 82 (21), 10341–10348.
Garry, C.E., Garry, R.F., 2004. Proteomics computational analyses suggest that the carboxyl terminal glycoproteins of Bunyaviruses are class II viral fusion protein (beta-penetrenes). Theor. Biol. Med. Model 1, 10.
Gerrard, S.R., Nichol, S.T., 2007. Synthesis, proteolytic processing and complex formation of N-terminally nested precursor proteins of the Rift Valley fever virus glycoproteins. Virology 357 (2), 124–133.
Huiskonen, J.T., Overby, A.K., Weber, F., Grunewald, K., in press. Electron Cryo-Microscopy and Single-Particle Averaging of Rift Valley Fever Virus: Evidence for GN-GC Glycoprotein Heterodimers. J. Virol. doi:10.1128/JVI.02483-08.
Ji, Y., Marinescu, D.C., Zhang, W., Zhang, X., Yan, X., Baker, T.S., 2006. A model-based parallel origin and orientation refinement algorithm for cryoTEM and its application to the study of virus structures. J. Struct. Biol. 154 (1), 1–19.
Liu, L., Celma, C.C., Roy, P., 2008. Rift Valley fever virus structural proteins: expression, characterization and assembly of recombinant proteins. Virol. J. 5, 82.
Ludtke, S.J., Baldwin, P.R., Chiu, W., 1999. EMAN: semiautomated software for high-resolution single-particle reconstructions. J. Struct. Biol. 128 (1), 82–97.
Matthews, B.W., 1968. Solvent content of protein crystals. J. Mol. Biol. 33 (2), 491–497.
Overby, A.K., Popov, V., Neve, E.P., Pettersson, R.F., 2006. Generation and analysis of infectious virus-like particles of Uukuniemi virus (*Bunyaviridae*): a useful system for studying bunyaviral packaging and budding. J. Virol. 80 (21), 10428–10435.
Overby, A.K., Pettersson, R.F., Neve, E.P., 2007. The glycoprotein cytoplasmic tail of Uukuniemi virus (*Bunyaviridae*) interacts with ribonucleoproteins and is critical for genome packaging. J. Virol. 81 (7), 3198–3205.
Overby, A.K., Pettersson, R.F., Grunewald, K., Huiskonen, J.T., 2008. Insights into bunyavirus architecture from electron cryotomography of Uukuniemi virus. Proc. Natl. Acad. Sci. U.S.A. 105 (7), 2375–2379.
Pettersen, E.F., Goddard, T.D., Huang, C.C., Couch, G.S., Greenblatt, D.M., Meng, E.C., Ferrin, T.E., 2004. UCSF chimera—a visualization system for exploratory research and analysis. J. Comput. Chem. 25 (13), 1605–1612.
Rey, F.A., Heinz, F.X., Mandl, C., Kunz, C., Harrison, S.C., 1995. The envelope glycoprotein from tick-borne encephalitis virus at 2 A resolution. Nature 375 (6529), 291–298.
Ronka, H., Hilden, P., Von Bonsdorff, C.H., Kuismanen, E., 1995. Homodimeric association of the spike glycoproteins G1 and G2 of Uukuniemi virus. Virology 211 (1), 241–250.
Rosenthal, P.B., Henderson, R., 2003. Optimal determination of particle orientation, absolute hand, and contrast loss in single-particle electron cryomicroscopy. J. Mol. Biol. 333 (4), 721–745.
Schmaljohn, C.S., Nichol, S.T., 2007. Bunyaviridae, In: Knipe, D.M., Howley, P.M. (Eds.), Fifth ed. Fields Virology, Vol. 2. Wolters Kluwer, Philadelphia, PA, pp. 1741–1790.
Shi, X., Kohl, A., Li, P., Elliott, R.M., 2007. Role of the cytoplasmic tail domains of Bunyamwera orthobunyavirus glycoproteins Gn and Gc in virus assembly and morphogenesis. J. Virol. 81 (18), 10151–10160.
Zhang, X., Walker, S.B., Chipman, P.R., Nibert, M.L., Baker, T.S., 2003. Reovirus polymerase lambda 3 localized by cryo-electron microscopy of virions at a resolution of 7.6 A. Nat. Struct. Biol. 10 (12), 1011–1018.